Наносистеми, наноматеріали, нанотехнології
Nanosistemi, Nanomateriali, Nanotehnologii
2025, т. 23, № 4, сс. 1059–1074
https://doi.org/10.15407/nnn.23.04.1059

PACS numbers: 61.46.Bc, 71.15.Mb, 73.22.-f, 81.05.Zx, 82.45.Yz, 82.47.Aa

In Situ Solid-State Hybrid Lithium-Ion (Boron, Aluminium, Gallium) Batteries with Efficient Energy Density Realized by a Simulated Anode of Silicon–Germanium Oxide Nanocomposite

Fatemeh Mollaamin

Department of Biomedical Engineering,
Faculty of Engineering and Architecture,
Kastamonu University,
Kastamonu, Turkey

As the energy density of commercial lithium (Li) ion batteries with graphite anode is low, a hybrid alloy of [Li-ion/boron (B), aluminium (Al), gallium (Ga)] battery is figured out by a simulated anode of germanium–silicon oxide (GeOSiO) and tin–silicon oxide (SnOSiO) nanoclusters. To be specific, a scalable simulated method is developed to fabricate the hybrid alloy of (GeOSiO) and (SnOSiO) nanoclusters, which acts as a smart anode nanocomposite for Li-ion intercalation and subsequent metalloid/metal of boron, aluminium and gallium due to the elevated lithiophilicity and efficient ion-conducting path. (GeOSiO) and (SnOSiO) nanoclusters have been designed and characterized as the electrodes for hybrid Li-ion batteries (LIBs) due to forming [LiB(GeOSiO)], [LiAl(GeOSiO)], [LiGa(GeOSiO)], [LiB(SnOSiO)], [LiAl(SnOSiO)], and [LiGa(SnOSiO)] nanoclusters. In this work, the metalloid/metal elements of third group have been studied in hybrid LiB-, LiAl-, LiGa-ion batteries through using computational approaches due to density-state analysis of charge-density differences (CDD), total density of state (TDOS), electron-localization function (ELF). Higher Ge/Sn to Si content can increase battery capacity for energy storage compared to net Li-ion batteries and might improve the rate performances by enhancing electrical conductivity. Besides, (GeOSiO) and (SnOSiO) anode materials may advance cycling consistency by excluding electrode decline and augments the capacity owing to higher surface capacitive impacts. To be specific, a scalable method is developed to fabricate the nanocomposite, which acts as a simulated anode for Li-ion intercalation and subsequent Li–metal/metalloid alloys owing to the enhanced lithiophilicity and sufficient ion-conducting pathways.

Оскільки густина енергії комерційних Літій-йонних акумуляторів (Li) з графітовою анодою є низькою, гібридний стоп [Літій+Бор (B), Алюміній (Al), Ґалій (Ga)]-йонного акумулятора було розраховано за допомо-

гою моделювання аноди з нанокластерів оксид Ґерманію–оксид Силіцію (GeO–SiO) та оксид Стануму–оксид Силіцію (SnOSiO). Зокрема, розроблено масштабований метод моделювання для виготовлення гібридного стопу нанокластерів (GeOSiO) та (SnOSiO), який діє як розумний анодний нанокомпозит для інтеркаляції йонів Літію та у подальшому металоїдів/металів (Бору, Алюмінію та Ґалію) завдяки підвищеній літіофільності й ефективному шляху йонної провідности. Нанокластери (GeOSiO) та (SnOSiO) було розроблено й охарактеризовано як електроди для гібридних Літій-йонних акумуляторів (LIB) завдяки утворенню нанокластерів [LiB(GeOSiO)], [LiAl(GeOSiO)], [LiGa(GeOSiO)], [LiB(SnOSiO)], [LiAl(SnOSiO)], [LiAl(SnOSiO)] та [LiGa(SnOSiO)]. У цій роботі досліджуються металоїдні/металічні елементи третьої групи в гібридних LiB-, LiAl-, LiGa-йонних акумуляторах за допомогою обчислювальних підходів, що ґрунтуються на аналізі ріжниць густин заряду (CDD), повних густин стану (TDOS), функцій локалізації електронів (ELF). Більш високий вміст Ge/Sn порівняно з Si може збільшити ємність акумулятора для накопичення енергії порівняно з чистими Літій-йонними акумуляторами та поліпшити швидкість заряду за рахунок підвищення електропровідности. Крім того, анодні матеріяли (GeOSiO) та (SnOSiO) можуть поліпшити циклічну стабільність, виключаючи виснаження електроди та збільшуючи ємність завдяки вищим поверхневим ємнісним впливам. Розроблено масштабований метод виготовлення нанокомпозиту, який діє як імітована анода для інтеркаляції йонів Літію й у подальшому стопів літію+металоїд/метал завдяки підвищеній літіофільності й достатній кількості шляхів провідности йонів.

Key words: nanocomposites, hybrid lithium/third-group ions' batteries, energy-saving, density of states, electrical conductivity.

Ключові слова: нанокомпозити, гібридні батареї літій–йони третьої групи, енергозбереження, густина станів, електропровідність.

(Received 12 June, 2025)

1. INTRODUCTION

It is relevant to remark that Si-based inorganic compounds have been extensively examined for lithium-ion batteries (LIBs) [1]. Similarly, although Si-based polymer-derived ceramics (PDCs) have already been investigated as electrodes in rechargeable LIBs [2], there are no results to discover their potential for magnesium-ion batteries (MIBs). One hopping anode material for LIBs is silicon (Si), with a theoretical capacity nearly ten times that of graphite [3]. However, the usage of Si-anodes remains moderate because of magnificent volume expansion and pulverization during battery cycling, conducting to structural deterioration and poor performance stability [1]. The extracted polymers from ceramics, especially with silicon backbone, might be a supreme candidate to modify the mentioned

concerns [2]. Therefore, SiOC with Si tetrahedrally co-ordinated to O and C has already been studied as electrodes in rechargeable lithium-ion batteries [4–7]. Moreover, Sn-containing SiOC/Sn nanobeads are synthesized with various C/Sn elements and examined as electrodes for Mg-ion batteries [8].

Owing to low electrical conductivity, additives such as tin (Sn) are provided to ameliorate the cycling consistency, rate performance of SiOC electrodes and reversible capacity [9, 10]. It should also be underlined that, like silicon electrodes, metallic tin electrodes endure severe volume expansion and particle association, conducting to poor cycling consistency [11]. Therefore, SiOC ceramics are appropriate active matrices to buffer volume alteration and density of tin during battery cycling [12–15].

Lately, the carbide hybrid nanomaterials of Si-, Ge-, and Sn have been proposed as occupied H_2-capture substances [16–18]. Whereas the polarizability of Si is more than C atom, it is assumed that Si–C/Si nanosurface may append to compositions more intensely in hybrid to the pure C-nanostructures [19–21]. The previous investigations of energy-saving devices through H-adsorption have been tailored owing to DFT calculations with a semiconductor group of Si/Ge/Sn/Pb nanocarbides [22], Mg–Al nanoalloy [23] and Al/C/Si doping of BN nanocomposite [24]. Nanomaterials with notable structures detect undertaking demands in the field of electrocatalysis, fuel cells, and energy-saving [25].

Recently, due to their unique electronic structures and hybrid forms, boron-based materials have been widely used in different lithium battery (LB) components, such as electrodes, electrolytes, separators, additives, and binders, to resolve these problems. Finally, some new strategies and perspectives on the application of boron in LB materials are proposed. Here, the aim is to provide a clear insight on the study of boron in energy storage materials and contribute to the promotion of further research in this area [26].

Because of the high capacity, natural abundance, and safety of aluminium (Al), the Al–Li alloy formed by combining it with lithium (Li) is an attractive anode material. So, the scientists proposed a new type of lithium battery that works in an open system and does not require sealing, the 'Lithium–Aluminium' soft pack battery (LAB). Compared to traditional lithium metal batteries (LMBs), their work demonstrated superior cycle stability, a safer operational environment, increased versatility in application scenarios, and reduced costs [27]. In addition, in a recent review, the developments on Ga-based LMs applied in LIBs have been discussed, including from the aspects of anodes, cathodes, and electrolytes [28].

The present investigation wants to delve into the feasibility of germanium–silicon oxide (GeOSiO) or tin–silicon oxide (SnOSiO)

nanocluster for B, Al, Ga-substitution with Li atom in [LiLi(GeOSiO)] or [LiLi(SnOSiO)] heterocluster and formation of [LiB(GeOSiO)], [LiAl(GeOSiO)], [LiGa(GeOSiO)], [LiB(SnOSiO)], [LiAl(SnOSiO)], and [LiGa(SnOSiO)] nanoclusters.

Therefore, it was analysed the physicochemical properties of mentioned heteroclusters of [LiLi(GeOSiO)], [LiB(GeOSiO)], [LiAl(GeOSiO)], [LiGa(GeOSiO)], [LiLi(SnOSiO)], [LiB(SnOSiO)], [LiAl(SnOSiO)], and [LiGa(SnOSiO)] nanoclusters. Regarding this context, (GeOSiO) or (SnOSiO) nanocluster was modelled with hybrid alkali metal of Li and third-group metalloid/metal of B/Al/Ga as cathode materials for comparison.

Following in-depth characterization, samples were measured for their performance correlated with chemical composition variations to legislate their potency for the first time in hybrid Li-batteries. Subsequently, the recent research progress on the application of B, Al, Ga in each component of the LB is summarized, aiming to understand the hybrid forms of B, Al, Ga and their potential for use in LB materials. Here, the aim is to provide a clear insight on the study of hybrid battery cells in energy storage materials and contribute to the promotion of further research in this area.

2. THEORY, MATERIALS AND COMPUTATION

Figure 1, *a*–*f* has shown hybrid lithium-(boron, aluminium, gallium) nanoclusters including [LiB(GeOSiO)], [LiAl(GeOSiO)], [LiGa(GeOSiO)], [LiB(SnOSiO)], [LiAl(SnOSiO)], and [LiGa(SnOSiO)] nanoclusters which can enhance energy-saving in [LiLi(GeOSiO)] or [LiLi(SnOSiO)] battery cells, transistors or other semiconducting devices.

In this investigation, the computations have been launched by Coulomb-attenuating method–(Becke, 3-parameter, Lee–Yang–Parr) [CAM–B3LYP–D3] level of theory. Figure 1, *a*–*f* indicates the status of producing [LiB(GeOSiO)], [LiAl(GeOSiO)], [LiGa(GeOSiO)], [LiB(SnOSiO)], [LiAl(SnOSiO)], and [LiGa(SnOSiO)] nanoclusters from [LiLi(GeOSiO)] or [LiLi(SnOSiO)] after Li-replacement with B, Al, Ga elements.

The analysis of Bader charge parameter [29] has been illustrated for [LiLi(GeOSiO)], [LiB(GeOSiO)], [LiAl(GeOSiO)], [LiGa(GeOSiO)], [LiB(SnOSiO)], [LiLi(SnOSiO)], [LiAl(SnOSiO)], and [LiGa(SnOSiO)] nanoclusters (Fig. 1, *a*–*f*) due to Gaussian 16 revision C.01 computational software [30] and GaussView 6.1 graphical program [31]. The applied basis sets for theoretical optimization of [LiLi(GeOSiO)], [LiB(GeOSiO)], [LiAl(GeOSiO)], [LiGa(GeOSiO)], [LiB(SnOSiO)], [LiLi(SnOSiO)], [LiAl(SnOSiO)], and [LiGa(SnOSiO)] nanoclusters have been supported by LANL2DZ and 6–311+G (*d*, *p*).

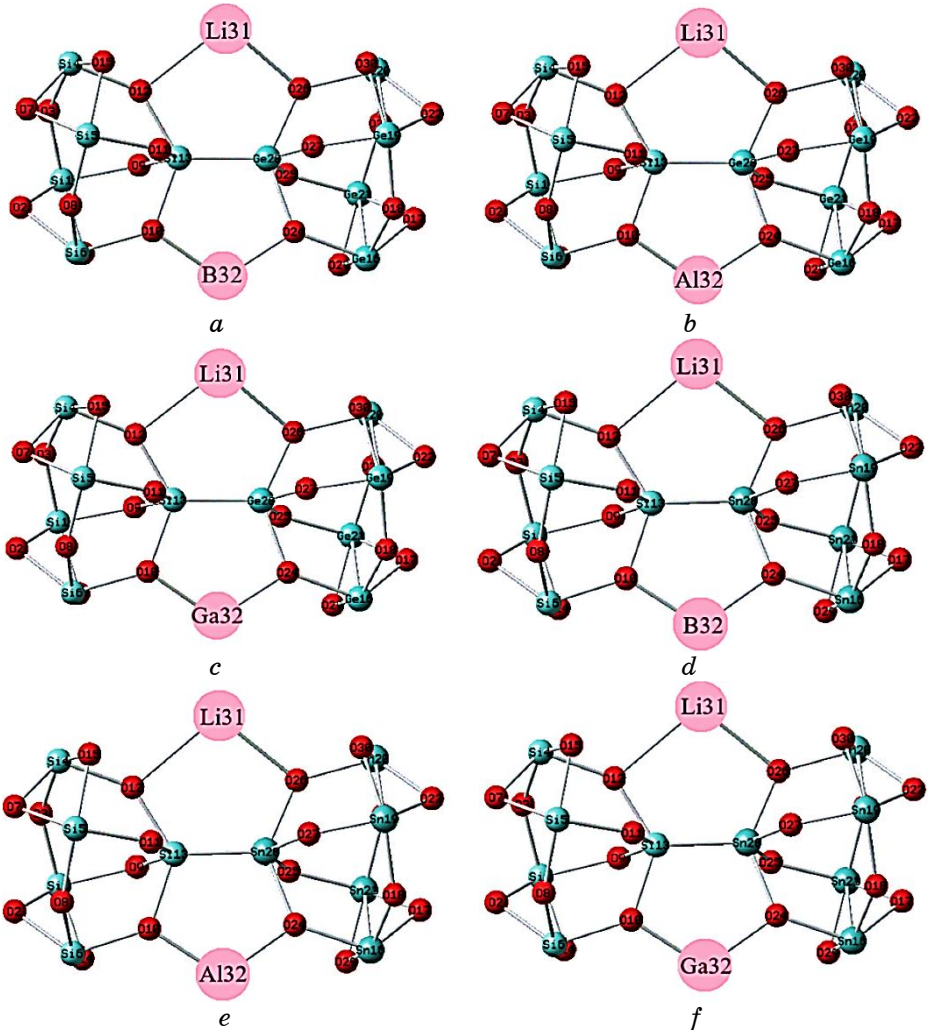

Fig. 1. Substituting of B, Al, Ga elements with Li element in [LiLi(GeOSiO)] or [LiLi(SnOSiO)] nanocluster and formation of (*a*) [LiB(GeOSiO)], (*b*) [LiAl(GeOSiO)], (*c*) [LiGa(GeOSiO)], (*d*).

One of the most significant advantages of applying (Ge/Sn)-containing SiO nanocluster as anodes/cathodes in lithium batteries is they provide several potential B/Al/Ga ion storage ways in a stable (GeOSiO) or (GeOSiO) anode material, increased electrical conductivity from Ge/Sn and surface area from the nanocluster morphology. In this investigation, homogenously distributed germanium or tin elements can be immobilized in the SiO matrix, which prevents their tendency to form agglomeration under battery cy-

cling. The B/Al/Ga insertion might also result in the cleavage of some Si–O, Ge–O or Sn–O bonds in the (GeOSiO) or (GeOSiO) anode material and the expansion, providing favourable sites for the subsequent ion insertion in the network. At the same time, B/Al/Ga atoms could react rapidly with a metalloid germanium or metal tin, and possibly oxide of (GeOSiO) or (GeOSiO) to produce different hybrid LiB-, LiAl-, LiGa-based alloys of [LiB(GeOSiO)] (Fig. 1, *a*), [LiAl(GeOSiO)] (Fig. 1, *b*), [LiGa(GeOSiO)] (Fig. 1, *c*), [LiB(SnOSiO)] (Fig. 1, *d*), [LiAl(SnOSiO)] (Fig. 1, *e*), and [LiGa(SnOSiO)] nanoclusters (Fig. 1, *f*).

3. RESULTS AND DISCUSSION

3.1. Charge Density Differences Analysis

In Figure 2, *a*–*c*, charge density differences (CDD) [32] have been shown for [LiB(GeOSiO)], [LiAl(GeOSiO)], and [LiGa(GeOSiO)] with the vibration in the range about –12 to +7 Bohr.

Moreover, the elements of O_2, O_3, O_7–O_{12}, O_{14}, O_{15}, O_{17}, $O_{(18)}$, O_{22}–O_{27}, O_{29}, O_{30} from Li*X*-based (*X* = B, Al, Ga) alloys have displayed the vibration about –12 to +8 Bohr for [LiB(SnOSiO)], [LiAl(SnOSiO)], and [LiGa(SnOSiO)] nanoclusters (Fig. 2, *d*–*f*).

The charge difference has been illustrated during substitution of Li atoms with B, Al or Ga in (GeOSiO) or (SnOSiO) nanocluster. Li-replacement by B, Al or Ga in [LiLi(GeOSiO)] with –1.631 coulomb produces [LiB(GeOSiO)], [LiAl(GeOSiO)], and [LiGa(GeOSiO)] with –1.601, –1.559, and –1.595 coulomb (Table 1). Moreover, Li-replacement by B, Al or Ga in [LiLi(SnOSiO)] with –1.785 coulomb builds [LiB(SnOSiO)], [LiAl(SnOSiO)], and [LiGa(SnOSiO)] with –1.729, –1.713, and –1.716 coulomb (Table 2).

Regarding the amounts of charge distribution, functionalizing of B, Al, Ga atoms can augment the negative atomic charge of O_2, O_3, O_7–O_{12}, O_{14}, O_{15}, O_{17}, $O_{(18)}$, O_{22}–O_{27}, O_{29}, O_{30} in [Li*X*(SnOSiO)] (*X* = B, Al, Ga) more than [Li*X*(GaOSiO)] (*X* = B, Al, Ga) complex.

In fact, [LiB(SnOSiO)], [LiAl(SnOSiO)], and [LiGa(SnOSiO)] hybrid nanoclusters have displayed more output than [LiB(GeOSiO)], [LiAl(GeOSiO)] and [LiGa(GeOSiO)] [32] for electron acceptance during Li-replacement (Tables 1 and 2).

3.2. Total Density of State

In isolated system (such as molecule), the energy levels are discrete, the concept of 'density of state (DOS)' is supposed to be completely valueless in this situation. Therefore, the 'original total DOS

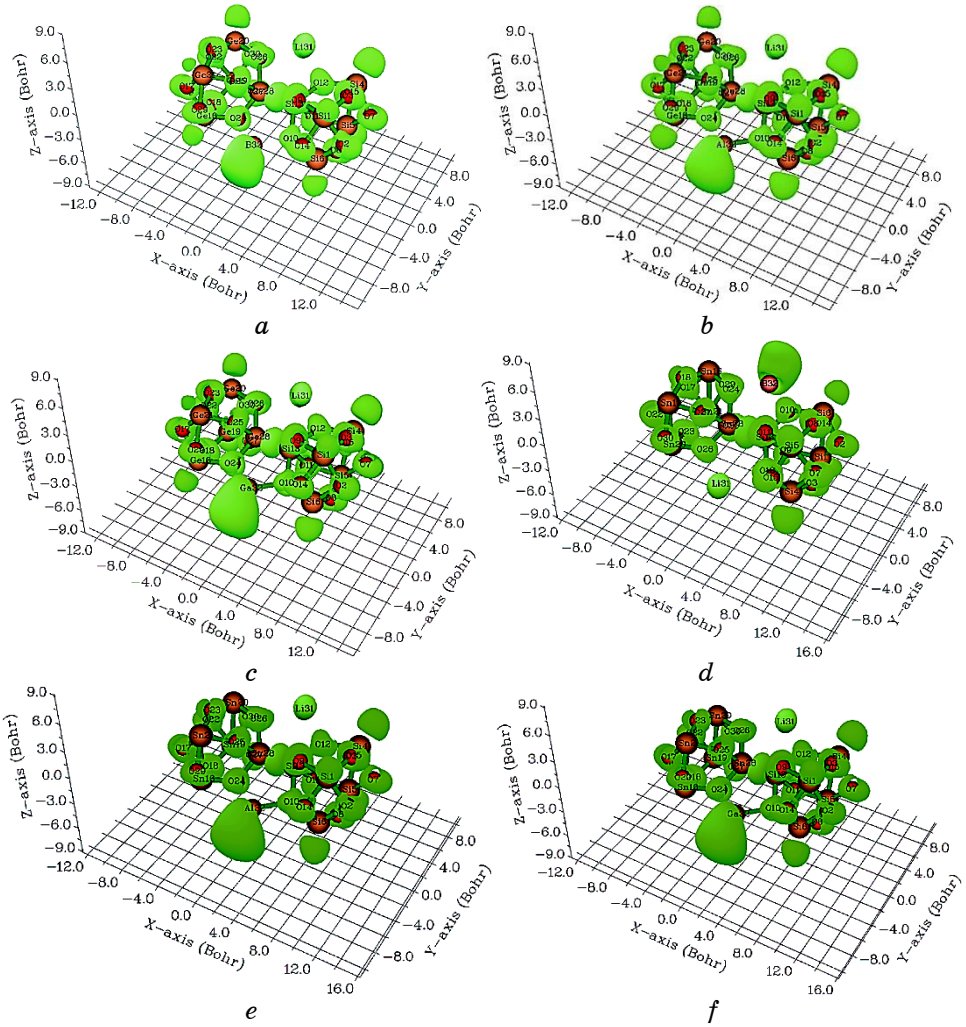

Fig. 2. CDD graphs for (*a*) [LiB(GeOSiO)], (*b*) [LiAl(GeOSiO)], (*c*) [LiGa(GeOSiO)], (*d*) [LiB(SnOSiO)], (*e*) [LiAl(SnOSiO)], and (*f*) [LiGa(SnOSiO)] nanoclusters.

(TDOS)' of isolated system can be written as [33]:

$$\mathrm{TDOS}(E) = \sum_i \delta\left(E - \in_i\right). \tag{1}$$

The normalized Gaussian function is defined as follows:

$$G(x) = \frac{1}{c\sqrt{2\pi}} e^{-\frac{x^2}{2c^2}}, \text{ where } c = \frac{FWHM}{2\sqrt{2\ln x}}. \tag{2}$$

'*FWHM* (full width at half maximum)' is an adjustable parameter in 'Multiwfn' [34, 35]. Furthermore, the curve maps of 'broadened partial DOS (PDOS)' and 'overlap DOS (OPDOS)' are valuable for visualizing orbital composition analysis, 'PDOS function of

TABLE 1. The atomic charge [*Q*/coulomb] for [LiLi(GeOSiO)], [LiB(GeOSiO)], [LiAl(GeOSiO)] and [LiGa(GeOSiO)] nanoclusters.

[LiLi(GeOSiO)]		[LiB(GeOSiO)]		[LiAl(GeOSiO)]		[LiGa(GeOSiO)]	
Atom	*Q*	Atom	*Q*	Atom	*Q*	Atom	*Q*
Si1	1.46	Si1	1.47	Si1	1.46	Si1	1.46
O2	–0.68	O2	–0.62	O2	–0.66	O2	–0.64
O3	–0.83	O3	–0.83	O3	–0.83	O3	–0.83
Si4	1.43	Si4	1.44	Si4	1.43	Si4	1.43
Si5	1.46	Si5	1.45	Si5	1.44	Si5	1.44
Si6	1.46	Si6	1.51	Si6	1.45	Si6	1.48
O7	–0.65	O7	–0.71	O7	–0.68	O7	–0.70
O8	–0.83	O8	–0.84	O8	–0.85	O8	–0.84
O9	–0.80	O9	–0.78	O9	–0.80	O9	–0.79
O10	–1.01	O10	–0.90	O10	–1.10	O10	–1.06
O11	–0.80	O11	–0.82	O11	–0.82	O11	–0.82
O12	–0.94	O12	–0.95	O12	–0.94	O12	–0.95
Si13	1.63	Si13	1.60	Si13	1.56	Si13	1.59
O14	–0.70	O14	–0.75	O14	–0.75	O14	–0.77
O15	–0.76	O15	–0.69	O15	–0.72	O15	–0.70
Ge16	1.39	Ge16	1.43	Ge16	1.39	Ge16	1.41
O17	–0.67	O17	–0.61	O17	–0.65	O17	–0.62
O18	–0.78	O18	–0.78	O18	–0.78	O18	–0.78
Ge19	1.38	Ge19	1.39	Ge19	1.38	Ge19	1.38
Ge20	1.39	Ge20	1.38	Ge20	1.38	Ge20	1.38
Ge21	1.39	Ge21	1.41	Ge21	1.40	Ge21	1.40
O22	–0.62	O22	–0.69	O22	–0.66	O22	–0.70
O23	–0.78	O23	–0.80	O23	–0.79	O23	–0.79
O24	–0.94	O24	–0.85	O24	–1.03	O24	–0.99
O25	–0.80	O25	–0.77	O25	–0.80	O25	–0.79
O26	–0.92	O26	–0.91	O26	–0.91	O26	–0.91
O27	–0.77	O27	–0.81	O27	–0.81	O27	–0.81
Ge28	1.24	Ge28	1.22	Ge28	1.21	Ge28	1.22
O29	–0.69	O29	–0.73	O29	–0.73	O29	–0.76
O30	–0.73	O30	–0.66	O30	–0.69	O30	–0.67
Li31	0.73	Li31	0.76	Li31	0.74	Li31	0.75
Li32	0.74	B32	0.48	Al32	1.19	Ga32	0.98

TABLE 2. The atomic charge [Q/coulomb] for [LiLi(SnOSiO)], [LiB(SnOSiO)], [LiAl(SnOSiO)] and [LiGa(SnOSiO)] nanoclusters.

[LiLi(SnOSiO)]		[LiB(SnOSiO)]		[LiAl(SnOSiO)]		[LiGa(SnOSiO)]	
Atom	Q	Atom	Q	Atom	Q	Atom	Q
Si1	1.45	Si1	1.46	Si1	1.45	Si1	1.45
O2	–0.63	O2	–0.63	O2	–0.69	O2	–0.69
O3	–0.83	O3	–0.83	O3	–0.83	O3	–0.83
Si4	1.41	Si4	1.42	Si4	1.42	Si4	1.42
Si5	1.43	Si5	1.44	Si5	1.44	Si5	1.44
Si6	1.47	Si6	1.50	Si6	1.46	Si6	1.47
O7	–0.72	O7	–0.72	O7	–0.67	O7	–0.67
O8	–0.83	O8	–0.84	O8	–0.84	O8	–0.83
O9	–0.78	O9	–0.78	O9	–0.81	O9	–0.80
O10	–1.00	O10	–0.90	O10	–1.10	O10	–1.05
O11	–0.81	O11	–0.82	O11	–0.83	O11	–0.83
O12	–0.95	O12	–0.94	O12	–0.93	O12	–0.93
Si13	1.41	Si13	1.37	Si13	1.37	Si13	1.37
O14	–0.76	O14	–0.75	O14	–0.73	O14	–0.72
O15	–0.69	O15	–0.69	O15	–0.77	O15	–0.77
Sn16	1.69	Sn16	1.73	Sn16	1.71	Sn16	1.71
O17	–0.81	O17	–0.81	O17	–0.81	O17	–0.81
O18	–0.88	O18	–0.88	O18	–0.88	O18	–0.88
Sn19	1.69	Sn19	1.71	Sn19	1.70	Sn19	1.70
Sn20	1.66	Sn20	1.70	Sn20	1.68	Sn20	1.70
Sn21	1.69	Sn21	1.71	Sn21	1.71	Sn21	1.71
O22	–0.84	O22	–0.84	O22	–0.84	O22	–0.84
O23	–0.89	O23	–0.89	O23	–0.89	O23	–0.89
O24	–1.04	O24	–0.94	O24	–1.11	O24	–1.07
O25	–0.90	O25	–0.90	O25	–0.92	O25	–0.92
O26	–1.00	O26	–1.00	O26	–1.00	O26	–1.00
O27	–0.94	O27	–0.95	O27	–0.95	O27	–0.95
Sn28	1.78	Sn28	1.71	Sn28	1.69	Sn28	1.71
O29	–0.88	O29	–0.87	O29	–0.89	O29	–0.89
O30	–0.86	O30	–0.86	O30	–0.86	O30	–0.86
Li31	0.70	Li31	0.72	Li31	0.71	Li31	0.71
Li32	0.68	B32	0.40	Al32	1.03	Ga32	0.85

fragment A' is defined as

$$\mathrm{PDOS}_A(E) = \sum_i \Xi_{i,A} F\left(E - \in_i\right), \tag{3}$$

where '$\Xi_{i,A}$ is the composition of fragment A in orbital i'.

The 'OPDOS between fragment A and B' is defined as

$$\mathrm{OPDOS}_{A,B}(E) = \sum_i X^i_{A,B} F\left(E - \in_i\right), \tag{4}$$

where '$X^i_{A,B}$ is the composition of total cross term between fragment A and B in orbital I'.

In the 'TDOS map', each discrete vertical line corresponds to a 'molecular orbital (MO)', the dashed line highlights the position of 'HOMO'. The curve is the 'TDOS' simulated based on the distribu-

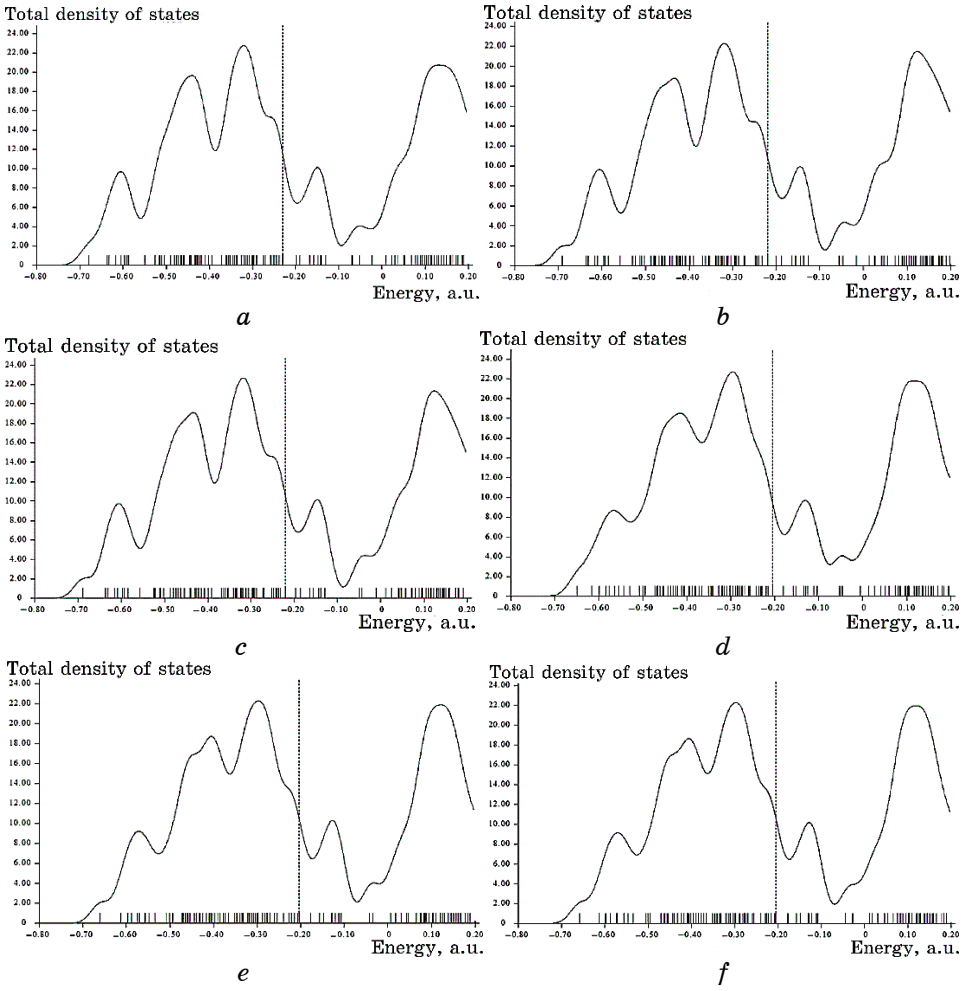

Fig. 3. TDOS graphs of (*a*) [LiB(GeOSiO)], (*b*) [LiAl(GeOSiO)], (*c*) [LiGa(GeOSiO)], (*d*) [LiB(SnOSiO)], (*e*) [LiAl(SnOSiO)], and (*f*) [LiGa(SnOSiO)] nanoclusters.

tion of 'MO' energy levels.

Regarding Li-replacement and producing [LiB(GeOSiO)], [LiAl(GeOSiO)], [LiGa(GeOSiO)], [LiB(SnOSiO)], [LiAl(SnOSiO)], and [LiGa(SnOSiO)] nanoclusters, TDOS has been evaluated. This factor can demonstrate the existence of important chemical interactions often on the 'convex side' (Fig. 3, *a*–*f*).

LiB(GeOSiO)], [LiAl(GeOSiO)], [LiGa(GeOSiO)] (Fig. 3, *a*–*c*) have shown the steepest maximums TDOS surrounding –0.30, –0.40 and –0.60 a.u. owing to covalent bond between Li/B, Li/Al and Li/Ga with (GeOSiO) nanocluster with maximum density of state of ≈ 22. However, LiB(SnOSiO)], [LiAl(SnOSiO)], [LiGa(SnOSiO)] (Fig. 3, *d*–*f*) have shown the steepest maximums TDOS surrounding –0.30, –0.40, –0.45 and –0.60 a.u. owing to covalent bond between Li/B, Li/Al and Li/Ga with (GeOSiO) nanocluster.

3.3. Electron-Localization Function Analysis

A type of scalar fields called ELF may demonstrate a broad span of bonding samples. Nevertheless, the distinction between deduced/raised electron delocalization/localization into cyclic π-conjugated sets stays encouraging for ELF [36].

The grosser the electron localization is in an area, the more likely the electron movement is restricted within it. Therefore, they might be discerned from the ones away if electrons are totally centralized. As Bader investigated, the zones with large electron localization possess extensive magnitudes of Fermi hole integration [37].

However, with having a six-dimension function for the Fermi hole, it seems hard to be studied directly. Then, Becke and Edgecombe remarked that spherically averaged-like spin conditional pair probability possesses a direct correlation with the Fermi hole and proposed the parameter of ELF in 'Multiwfn' program [34, 35] and popularized for spin-polarized procedure [38]. Regarding kinetic energy, ELF was rechecked to be more punctual for both Kohn–Sham DFT and post-HF wave functions [39].

Li-replacement in [LiLi(GeOSiO)] and [LiLi(SnOSiO)] towards formation of [LiB(GeOSiO)], [LiAl(GeOSiO)], [LiGa(GeOSiO)], [LiB(SnOSiO)], [LiAl(SnOSiO)], and [LiGa(SnOSiO)] nanoclusters might be described by ELF graphs using 'Multiwfn' [34, 35] due to achieving their delocalization/localization characterizations [36] of electrons and chemical bonds (Fig. 4, *a*–*f*). [LiB(GeOSiO)] (Fig. 4, *a*), [LiAl(GeOSiO)] (Fig. 4, *b*), [LiGa(GeOSiO)] (Fig. 4, *c*), [LiB(SnOSiO)] (Fig. 4, *d*), [LiAl(SnOSiO)] (Fig. 4, *e*), and [LiGa(SnOSiO)] nanoclusters (Fig. 4, *f*) have demonstrated the electron delocalization through an isosurface map with labelling atoms of O_{10}, O_{12}, Si_{13}, O_{24}, O_{26}, Ge_{28} or Sn_{28}, $X_{(31)}$ (X = Li), and $Y_{(32)}$ (Y = B, Al or Ga).

In fact, the counter map of ELF can confirm that (GeOSiO) and

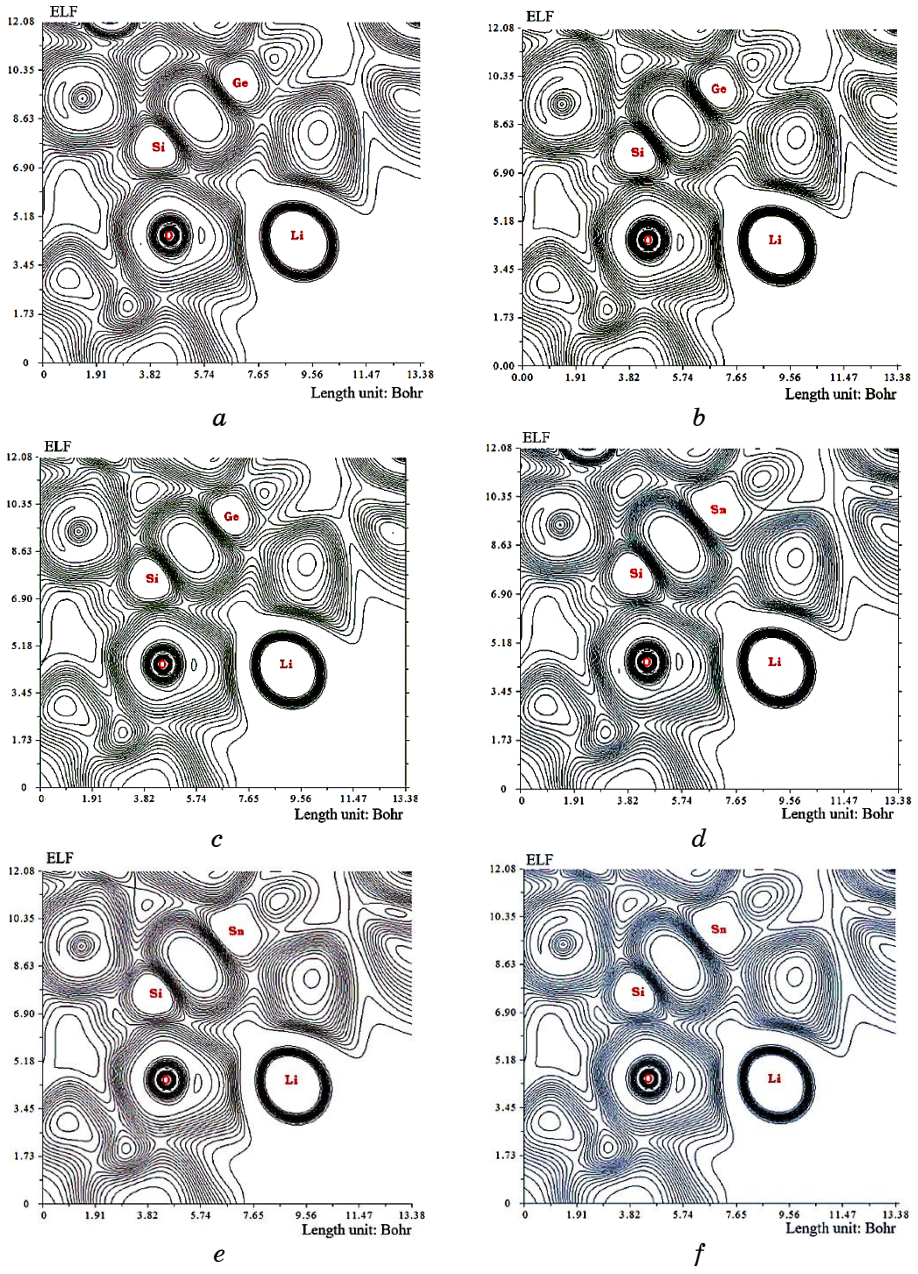

Fig. 4. The shaded map of ELF graphs for (*a*) [LiB(GeOSiO)], (*b*) [LiAl(GeOSiO)], (*c*) [LiGa(GeOSiO)], (*d*) [LiB(SnOSiO)], (*e*) [LiAl(SnOSiO)], and (*f*) [LiGa(SnOSiO)] nanoclusters.

TABLE 3. Stability energy (kcal/mole), dipole moment (Debye), LUMO (eV), HOMO (eV), and energy gap (ΔE) (eV) for [LiLi(GeOSiO)], [LiB(GeOSiO)], [LiAl(GeOSiO)], [LiGa(GeOSiO)], [LiLi(SnOSiO)], [LiB(SnOSiO)], [LiAl(SnOSiO)], and [LiGa(SnOSiO)] heteroclusters.

Heteroclusters	$E_s \cdot 10^{-3}$, kcal/mole	Dipole moment, Debye	E_{HOMO}, eV	E_{LUMO}, eV	$\Delta E = E_{LUMO} - E_{HOMO}$, eV
[LiLi(GeOSiO)]	–976.6396	1.9540	–6.08	–5.17	0.90
[LiB(GeOSiO)]	–987.3651	5.1019	–6.2684	–5.4033	0.8651
[LiAl(GeOSiO)]	–973.1316	2.7896	–5.9808	–5.4486	0.5322
[LiGa(GeOSiO)]	–973.1647	3.5806	–6.0128	–5.3555	0.6573
[LiLi(SnOSiO)]	–975.0148	5.18	–5.36	–4.70	0.6512
[LiB(SnOSiO)]	–985.7417	7.2925	–5.5745	–4.9322	0.6422
[LiAl(SnOSiO)]	–971.5038	6.9703	–5.5441	–4.8167	0.7274
[LiGa(SnOSiO)]	–971.5367	6.8634	–5.5671	–4.8268	0.7436

(SnOSiO) heteroclusters may augment the efficiency during formation of [LiB(GeOSiO)], [LiAl(GeOSiO)], [LiGa(GeOSiO)], [LiB(SnOSiO)], [LiAl(SnOSiO)], and [LiGa(SnOSiO)] nanoclusters (Tables 1, 2). Besides, intermolecular orbital overlap integral is important in illustration of intermolecular charge transfer, which can compute the HOMO–HOMO and LUMO–LUMO overlap integrals between the lithium and third-group elements of boron, aluminium, gallium in [LiB(GeOSiO)], [LiAl(GeOSiO)], [LiGa(GeOSiO)], [LiB(SnOSiO)], [LiAl(SnOSiO)], and [LiGa(SnOSiO)] nanoclusters.

The layered germanium/tin-silicon oxide improved by hybrid litium and third group metalloid/metal elements of boron, aluminium, gallium have indicated the structural stability of LiB-, LiAl-, LiGa-ion batteries through the reported stability energy in Table 3 and Fig. 5. In fact, a small portion of B, Al or Ga entered the Si–Ge or Si–Sn layer of [LiLi(GeOSiO)] or [LiLi(SnOSiO)] to replace lithium site with third-group metalloid/metal elements might improve the structural stability of the electrode material at high multiplicity, thereby, improving the capacity retention rate.

4. CONCLUSIONS

Li-replacement in [LiLi(GeOSiO)] and [LiLi(SnOSiO)] towards for-

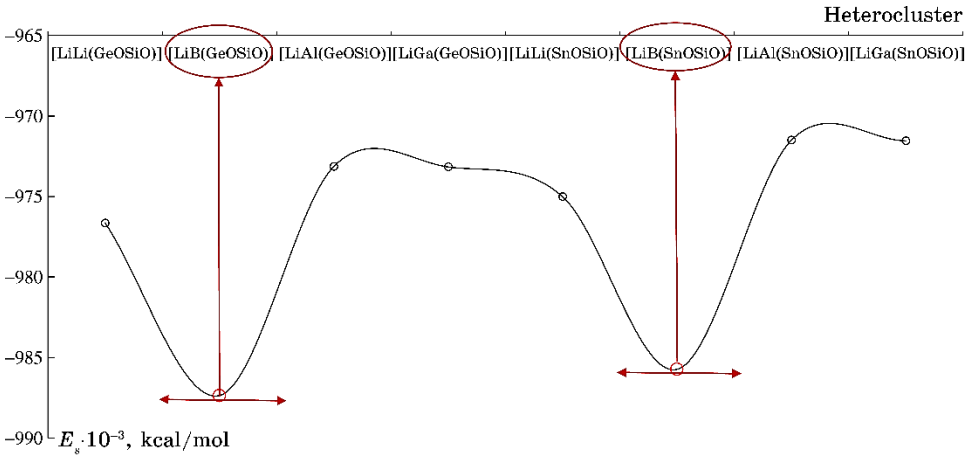

Fig. 5. The graph of stability energy (E_s, kcal/mole) for (*a*) [LiB(GeOSiO)], (*b*) [LiAl(GeOSiO)], (*c*) [LiGa(GeOSiO)], (*d*) [LiB(SnOSiO)], (*e*) [LiAl(SnOSiO)], and (*f*) [LiGa(SnOSiO)] nanoclusters.

mation of [LiB(GeOSiO)], [LiAl(GeOSiO)], [LiGa(GeOSiO)], [LiB(SnOSiO)], [LiAl(SnOSiO)] and [LiGa(SnOSiO)] nanoclusters was studied by computational method. The changes of charge density defined a notable charge transfer in nanoclusters of [LiB(SnOSiO)], [LiAl(SnOSiO)], [LiGa(SnOSiO)] than [LiB(GeOSiO)], [LiAl(GeOSiO)], [LiGa(GeOSiO)]. It is well established that adding of B, Al or Ga to Li-cell batteries might augment the energy-saving in cell batteries. Moreover, lithium replacing sites with B, Al or Ga in [LiB(GeOSiO)], [LiAl(GeOSiO)], [LiGa(GeOSiO)], [LiB(SnOSiO)], [LiAl(SnOSiO)], [LiGa(SnOSiO)] nanoclusters can alleviate parasitic saving of energy in hybrid LiB-, LiAl-, LiGa-ion batteries. The results of this research article represent that the architectural design of hybrid oxide nanoalloy of *XY*(GeOSiO) or *XY*(SnOSiO) (X = Li/Y = B, Al, Ga) can augment the capacity of battery cell.

The author is grateful to Kastamonu University for completing this paper and her research.

REFERENCES

1. Xiuyun Zhao and Vesa-Pekka Lehto, *Nanotechnology*, **32**, No. 4: 042002 (2021); https://doi.org/10.1088/1361-6528/abb850
2. Qingbo Wen, Fangmu Qu, Zhaoju Yu, Magdalena Graczyk-Zajac, Xiang Xiong, and Ralf Riedel, *J. Adv. Ceram.*, **11**: 984 (2022); https://doi.org/10.1007/s40145-022-0600-8
3. Mingzheng Ge, Chunyan Cao, Gill M. Biesold, Christopher D. Sewell, Shu-Meng Hao, Jianying Huang, Wei Zhang, Yuekun Lai, and Zhiqun Lin, *Adv. Mater.*, **33**:

2004577 (2021); https://doi.org/10.1002/adma.202004577
4. Gaofeng Shao, Dorian A. H. Hanaor, Jun Wang, Delf Kober, Shuang Li, Xifan Wang, Xiaodong Shen, Maged F. Bekheet, and Aleksander Gurlo, *ACS Appl. Mater. Interfaces*, **12**, Iss. 41: 46045 (2020); https://doi.org/10.1021/acsami.0c12376
5. Gabriela Mera, Alexandra Navrotsky, Sabyasachi Sen, Hans-Joachim Kleebe, and Ralf Riedel, *J. Mater. Chem. A*, **1**: 3826 (2013); https://doi.org/10.1039/c2ta00727d
6. Monika Wilamowska-Zawlocka, Paweł Puczkarski, Zofia Grabowska, Jan Kaspar, Magdalena Graczyk-Zajac, Ralf Riedel, and Gian D. Sorarù, *RSC Adv.*, **6**: 104597 (2016); https://doi.org/10.1039/C6RA24539K
7. V. S. Pradeep, D. G. Ayana, M. Graczyk-Zajac, G. D. Soraru, and R. Riedel, *Electrochim. Acta*, **157**: 41 (2015); https://doi.org/10.1016/j.electacta.2015.01.088
8. Wuqi Guo, Oyku Icin, Cekdar Vakifahmetoglu, Delf Kober, Aleksander Gurlo, and Maged F. Bekheet, *Adv. Funct. Mater.*, **33**: 2304933 (2023); doi:10.1002/adfm.202304933
9. Cheng Shi, Hui Huang, Yang Xia, Jiage Yu, Ruyi Fang, Chu Liang, Jun Zhang, Yongping Gan, and Wenkui Zhang, *Chemistry*, **25**, Iss. 32: 7719 (2019); https://doi.org/10.1002/chem.201900786
10. Kostiantyn Kravchyk, Loredana Protesescu, Maryna I. Bodnarchuk, Frank Krumeich, Maksym Yarema, Marc Walter, Christoph Guntlin, and Maksym V. Kovalenko, *J. Am. Chem. Soc.*, **135**, Iss. 11: 4199 (2013); https://doi.org/10.1021/ja312604r
11. Joseph Gonzalez, Ke Sun, Meng Huang, Shen Dillon, Ioannis Chasiotis, and John Lambros, *J. Power Sources*, **285**: 205 (2015); https://doi.org/10.1016/j.jpowsour.2015.03.093
12. Jun Wang, Delf Kober, Gaofeng Shao, Jan Dirk Epping, Oliver Gцrke, Shuang Li, Aleksander Gurlo, and Maged F. Bekheet, *Mater. Today Energy*, **26**: 100989 (2022); https://doi.org/10.1016/j.mtener.2022.100989
13. Romain J.-C. Dubey, Pradeep Vallachira Warriam Sasikumar, Frank Krumeich, Gurdial Blugan, Jakob Kuebler, Kostiantyn V. Kravchyk, Thomas Graule, and Maksym V. Kovalenko, *Adv. Sci.*, **6**, Iss. 19: 1901220 (2019); https://doi.org/10.1002/advs.201901220
14. Jan Kaspar, Caglar Terzioglu, Emanuel Ionescu, Magdalena Graczyk-Zajac, Stefania Hapis, Hans-Joachim Kleebe, and Ralf Riedel, *Adv. Funct. Mater.*, **24**: 4097 (2014); https://doi.org/10.1002/adfm.201303828
15. Duck Hyun Youn, Adam Heller, and C. Buddie Mullins, *Chem. Mater.*, **28**, Iss. 5: 1343 (2016); https://doi.org/10.1021/acs.chemmater.5b04282
16. Waqas Nazeer, Adeel Farooq, Muhammad Younas, Mobeen Munir, and Shin Min Kang, *Biomolecules*, **8**, Iss. 3: 92 (2018); https://doi.org/10.3390/biom8030092
17. Jiuzhou Zhao, Zhenjun Li, Matthew Thomas Cole, Aiwei Wang, Xiangdong Guo, Xinchuan Liu, Wei Lyu, Hanchao Teng, Yunpeng Qv, Guanjiang Liu, Ke Chen, Shenghan Zhou, Jianfeng Xiao, Yi Li, Chi Li, and Qing Dai, *Nanomaterials*, **11**, Iss. 12: 3244 (2021); https://doi.org/10.3390/nano11123244
18. Yaling Rong, Yali Cao, Nana Guo, Yizhao Li, Wei Jia, and Dianzeng Jia, *Electrochimica Acta*, **222**: 1691 (2016); https://doi.org/10.1016/j.electacta.2016.11.160
19. Nuttapon Yodsin, Hiroki Sakagami, Taro Udagawa, Takayoshi Ishimoto, Siriporn Jungsuttiwong, Masanori Tachikawa, *Molecular Catalysis*, **504**: 111486 (2021); https://doi.org/10.1016/j.mcat.2021.111486

20. Hayam Osman Taha, Atef M. El Mahdy, Fatma El Sayed El Shemy, and Mohammed Mohammed Hassan, *International Journal of Qantum Chemistry*, **123**, Iss. 3: e27023 (2023); https://doi.org/10.1002/qua.27023
21. Tao Wei, Yanyan Zhou, Cheng Sun, Xingtong Guo, Shoudong Xu, Daifen Chen and Yongfu Tang, *Nano Res.*, **17**: 2763 (2024); https://doi.org/10.1007/s12274-023-6187-8
22. F. Mollaamin and M. Monajjemi, *Russ. J. Phys. Chem. B*, **18**: 607 (2024); https://doi.org/10.1134/S1990793124020271
23. F. Mollaamin, S. Shahriari, and M. Monajjemi, *Russ. J. Phys. Chem. B*, **18**: 398 (2024); https://doi.org/10.1134/S199079312402026X
24. F. Mollaamin, *Russ. J. Phys. Chem. B*, **18**: 805 (2024); https://doi.org/10.1134/S1990793124700131
25. Haiying Che, Jing Liu, Hong Wang, Xiaoping Wang, Sheng S. Zhang, Xiao-Zhen Liao, and Zi-Feng Ma, *Electrochemistry Communications*, **83**: 20 (2017); doi.org/10.1016/j.elecom.2017.08.012
26. Longli Ma, Jian Tan, Yuan Wang, Zhu Liu, Yifan Yang, Tia Gray, Xiang Zhang, Mingxin Ye, and Jianfeng Shen, *Advanced Energy Materials*, **13**, Iss. 25: 2300042 (2023); doi.org/10.1002/aenm.202300042
27. Shuailiang Xu, Mingqiang Li, Haochen Weng, and Jingwen Li, *Inorganic Chemistry Communications*, **172**: 113783 (2025); doi.org/10.1016/j.inoche.2024.113783
28. Bin-Wei Zhang, Long Ren, Yun-Xiao Wang, Xun Xu, Yi Du, and Shi-Xue Dou, *Interdisciplinary Materials*, **1**, Iss. 3: 354 (2022); https://doi.org/10.1002/idm2.12042
29. G. Henkelman, A. Arnaldsson, and H. Jónsson, *Computational Materials Science*, 36, Iss. 3: 354 (2006).
30. M. J. Frisch, G. W. Trucks, H. B. Schlegel, G. E. Scuseria, M. A. Robb et al., *Gaussian 16, Revision C.01* (Wallingford CT.: Gaussian, Inc.: 2016).
31. GaussView, Version 6.06.16, Dennington, Roy; Keith, Todd A.; Millam, John M. Semichem Inc., Shawnee Mission, KS, 2016.
32. Zihan Xu, Chenglong Qin, Yushu Yu, Gang Jiang, and Liang Zhao, *AIP Advances*, **14**: 055114 (2024); https://doi.org/10.1063/5.0208082
33. Fatemeh Mollaamin and Majid Monajjemi, *New Materials, Compounds and Applications*, **8**, No. 3: 303 (2024); https://doi.org/10.62476/nmca83303
34. Tian Lu and Feiwu Chen, *J. Comput. Chem.*, **33**, Iss. 5: 580 (2012); https://doi.org/10.1002/jcc.22885
35. Tian Lu, *J. Chem. Phys.*, **161**: 082503 (2024); https://doi.org/10.1063/5.0216272
36. Chérif F. Matta, Paul W. Ayers, and Ronald Cook, *The Physics of Electron Localization and Delocalization. In: Electron Localization–Delocalization Matrices. Lecture Notes in Chemistry* (Cham: Springer: 2024), vol. **112**, p. 7–12; https://doi.org/10.1007/978-3-031-51434-0_2
37. Richard F. W. Bader, *Theor. Chem. Accounts: Theory, Comput., Modeling*, **105**: 276 (2001); https://doi.org/10.1007/s002140000233
38. A. D. Becke and K. E. Edgecombe, *J. Chem. Phys.*, **92**: 5397 (1990); https://doi.org/10.1063/1.458517
39. Andreas Savin, Ove Jepsen, Jürgen Flad, Ole Krogh Andersen, Heinzwerner Preuss, and Hans Georg von Schnering, *Angewandte Chemie Int. Edition English*, **31**, Iss. 2: 187 (1992); https://doi.org/10.1002/anie.199201871